JOURNAL OF MATERIALS SCIENCE **39** (2004) 2783–2788

Generation of metal and metal oxide nanoparticles by liquid flame spray process

J. M. MÄKELÄ, H. KESKINEN, T. FORSBLOM, J. KESKINEN
Aerosol Physics Laboratory, Institute of Physics, Tampere University of Technology, P.O. Box 692, FIN-33101, Tampere, Finland
E-mail: jyrki.makela@tut.fi

A liquid flame spray (LFS) process has been investigated for the generation of single component nanoparticles. In the LFS process, a solution consisting of metal nitrate dissolved in water is sprayed into a turbulent, high temperature H_2-O_2-flame. The primary spray droplets evaporate and subsequent reactions in the flame produce metal or metal oxide vapours which nucleate to final particulate form. In the study, the process characteristics were examined to produce 10–60 nm particles from silver, palladium and iron containing precursors. A systematic study using variable process parameters proved that the size of the generated nanoparticles is set by the mass flow rate of the metal precursor, only. The geometric standard deviation of the size distributions was seen to vary in a limited range of 1.35–1.4. The particle size was verified by aerosol instrumentation, the composition and morphology by X-ray diffraction (XRD) and transmission electron microscopy (TEM), correspondingly. The Ag and Pd particles were seen to consist of pure metals. For iron, the presence of all three of the following compounds were detected: Fe, Fe_2O_3 and Fe_3O_4.

1. Introduction

Nanoparticles, more specifically, particles with sizes less than 100 nm have been observed to have material properties different from the bulk, and they are very useful in modern material science and technology (e.g., [1–3]). Nanosized silver and palladium particles have several applications in electronics especially now that the electronic components are getting to nanoscale size. Nanometric scale silver, palladium and iron particles have many catalytic applications [3, 4] and nanosized iron oxide particles have applications in magnetic nanomaterials [5, 6]. These particles have been made by several aerosol techniques: spray pyrolysis, laser assisted pyrolysis, plasma spray and chemical vapour deposition [1, 3]. For all these methods, particle size and morphology of the powder play an important role. Also, relatively high production rates may be considered as advantageous.

Liquid flame spray (LFS) is a thermal particle production and coating technique originally developed for glass colouring [7, 8]. Also applications such as optical fibre fabrication or production of conductive alloys and catalytic materials can be considered. The advantages of the process are the large amount of particulate material produced, easy particle generation and flame control plus a large variety of available precursors to be atomised. Practically, almost any element that can be fed, in the form of a liquid solution, can be utilised to form nanoparticles by LFS. Experimental results on LFS characteristics were presented using aluminium nitrate ($Al(NO_3)_3 \cdot 9H_2O$) in isopropanol as a precursor [7]. In the study, both flame characteristics and primary droplet size of the spray were discussed. Liquid flame spraying of manganese nitrate, aluminium nitrate, aluminium isopropoxide, zirconium butoxcide and zirconium acetate, in both isopropanol and n-butanol solvent, was used to produce nanomaterial powders [9]. Both electron microscopy (TEM) and X-ray diffraction analysis (XRD) were used to obtain information about particle morphology and composition [9, 10]. A subsequent paper studied an advanced application of glass colouring [8]. As a result, particle size distribution in the size range 50 nm–10 μm was found to be bimodal, consisting of a fine and a coarse mode. The former was suggested to be formed by gas-to-particle conversion and the latter by conventional spray pyrolysis. The coarse mode particles were also analysed by X-ray diffraction. In those studies several parameters such as liquid feed rate and gas flow rate, were studied.

An overview of the particle production processes from liquid droplets to solid particles is presented in Fig. 1 [3]. The primary droplets (Mode 1) are partly or completely evaporated in the flame. The reaction of the precursor in the droplet phase leads to residual metal or metal oxide particles (Mode 2). The reaction and subsequent nucleation of the vaporised component produces the nucleation mode of nanosized particles (Mode 3). In the LFS process, the product particles consist of a dominant nucleation mode. Due to gas-to-particle conversion the nucleation mode has a relatively small standard deviation. Survival of residual particles

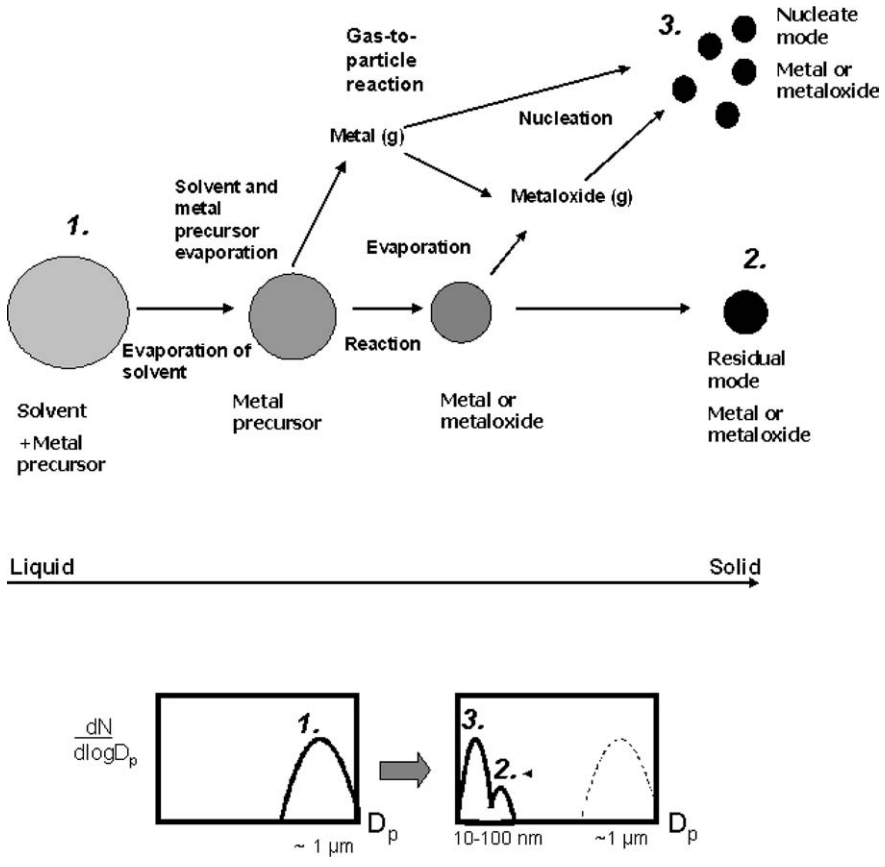

Figure 1 Overview of particle formation from liquid to solid by LFS-process (modified from [3]): 1. Primary spray droplets, 2. Spray pyrolysed residual particles and, 3. Nucleated nanoparticles from gas-to-particle conversion.

depends mostly on the vapour pressure and oxidation rate of the precursor. The particles have high production rate (g/min) which is proportional to the mass flow rate. In this paper, the production of silver, palladium and iron oxide particle by LFS is considered. The particle formation mechanism and influence of the mass flow rate on particle size in the LFS process have been studied. Also particle morphology has been studied by TEM and XRD.

2. Experimental equipment and method

The liquid flame spray (LFS) process is a method where the liquid precursor is atomised into small droplets, which are introduced into a H_2-O_2 flame. Evaporation of the liquid solvent droplets in the flame, followed by decomposition and re-condensation of product species, finally generates a well defined, nearly monodispersed nanoparticle material, to be sprayed on a surface or to be collected.

A schematic diagram of the LFS-process is shown in Fig. 2. The liquid precursor was fed into the spray gun atomiser with a manually controlled infusion pump. The selected precursors were nitrates of silver, iron and palladium. Precursor mass flow rate was controlled by setting the precursor concentration in the solvent and the liquid feed rate into the atomiser. A certain mass flow rate of precursor can be achieved with several combinations of precursor concentration and liquid feed rate. Various sets of runs using the concentration and precursor mass flow rate as the variable parameters were performed. Mass flow rates of 0.003–2 g/min (for the pure metal) have been used with O_2/H_2 flow rates of 40–80 l/min. Here, the precursors were $AgNO_3$-H_2O, $Pd(NH_3)_4NO_3$-H_2O and $FeNO_3 \cdot 9H_2O$-H_2O, but actual mass flow rates for pure metal are given in the text (e.g., for iron: $M(Fe)/M(FeNO_3 \cdot 9H_2O)$ times the precursor mass flow rate, where M is molar mass).

For producing nanoparticles from micrometre sized precursor droplets using LFS, in the ideal case, all of the material should be vaporised and, subsequently (either directly or via chemical reactions), nucleated and re-condensed. Fig. 3 shows a set of vapour pressure curves for the compounds in this study [11]. Melting points for silver, palladium and iron are 961.93, 1552 and 1535°C, and the boiling points are 2212, 3140 and

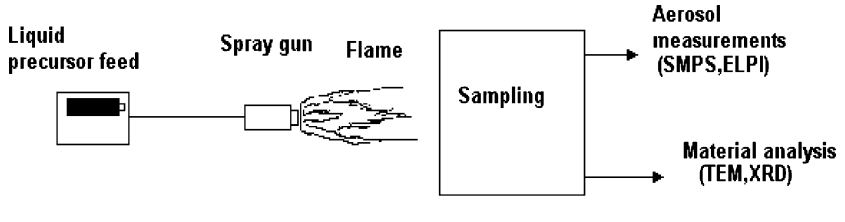

Figure 2 Schematic diagram of the LFS-process.

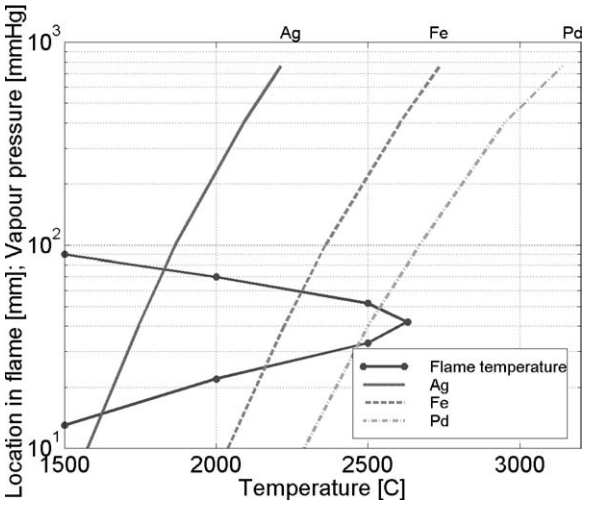

Figure 3 Equilibrium vapour pressure curves of the metal compounds used with the axial temperature profile of the flame.

2750°C, respectively. The boiling points can also be read from the upper ends of the vapour pressure curves (p_s = 760 mmHg,). Adapted from earlier work [7], also a typical axial temperature profile of the LFS flame is shown in Fig. 3. For palladium, the boiling point is well above the maximum temperature in the axis of the flame. In this case there is a doubt as to whether or not the material has time to be fully vaporised from the primary droplets. On the other hand the melting points of all these compounds are sufficiently low as to allow some extent of evaporation in the flame.

A specially designed patented spray gun modification [12] was used in the study. In the design used [9, 10], the atomiser was located in the centre of the gun head and two gas ducts were located as concentric rings around the atomiser so that the hydrogen duct was directly around the atomiser tube as shown in Fig. 4. The same oxygen flow acted as both fuel gas and atomising gas. A stoichiometric quantity of hydrogen was used in reaction with fuel gas. Gas flow rates were controlled manually according to rotameter and manometer readings. For hydrogen, flow rates of 80 l/min were used along with flow rates of 40 l/min for oxygen. The duration of each test run was of the order of one hour. The spray gun head was cleaned regularly to keep all the ducts uncontaminated and open.

The aerosol measurement experiments were carried out in an open-ended flow reactor sampling system. The thickness of the water cooled inner stainless steel shell of the reactor was 0.03 m. The length of the reactor was 0.6 m. The LFS gun is located at the top of the water-cooled cylindrical metal reactor (inner diameter 10 cm), shooting the flame downwards into the reactor. The reactor walls prevent excess oxygen flow from ambient air into the flame. Cooling is needed to avoid re-suspension from the reactor walls. An effective blower removes the exhaust gas from the bottom of the reactor. The sampling probe was located 0.40 m below the flame, at the bottom of the reactor. The sample flow was primarily diluted in the probe by a rotameter-controlled flow of heated compressed air. After primary dilution the sample was re-diluted in an ejector diluter [13], operating at a constant dilution ratio of 1/8. The sampling probe and the dilution system were connected by a 10 mm stainless steel tube. Excess flow was cooled in a water-filled container where the condensed droplets were separated.

The diluted sample was drawn into the three devices: Electrical Low Pressure Impactor (ELPI), Scanning Mobility Particle Sizer (SMPS) and point-to-plane electrostatic precipitator (TEM-collector). The electrical low pressure impactor [14] is based on particle pre-charging and aerodynamic size classification in the particle size range 30 nm–10 μm. The SMPS [15] measures number size distribution in the range 10–1000 nm due to electrical mobility of the particles. In the study a flow rate ratio of 0.6–6.0 l/min was used in SMPS. The combination of ELPI and SMPS can be used for the determination of the effective density of the particle [16]. For the measurement cycles, 5 s was used for ELPI and 5 min for SMPS. In addition to number size distribution measurement, particle samples were collected by a point-to-plane type single-stage electrostatic precipitator. This instrument uses a corona discharge to charge particles and collects particles by electrical forces on an electron microscope grid [17]. The grids were subsequently examined by Transmission Electron Microscopy (TEM).

For material analysis the particles were collected by using thermal force. The flame was directed to the water-cooled cylindrical metal reactor (inner diameter 0.15 m) of the same kind as the sampling system in the open-end reactor for aerosol measurement (shell thickness 1.5 cm and length 1.3 m). Particles were collected on the reactor walls and then rubbed off. The powder sample was analysed by X-ray diffraction (XRD).

3. Results and discussion

3.1. Particle synthesis

For the three compounds (Ag, Pd, Fe), the generated size distributions are close to log-normal shape with

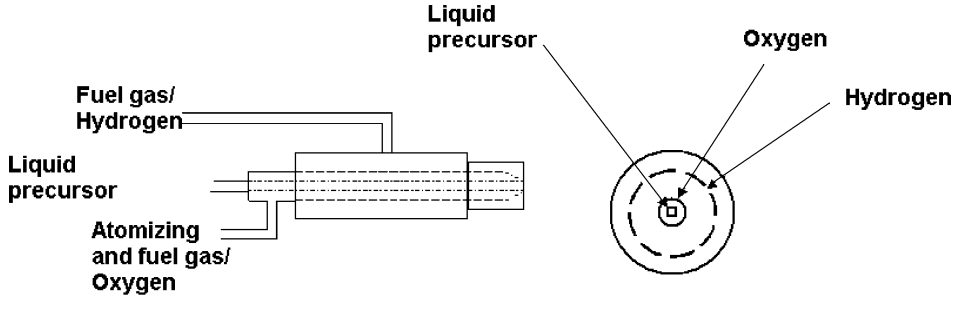

Figure 4 Schematic diagram of LFS-spray gun used in this study.

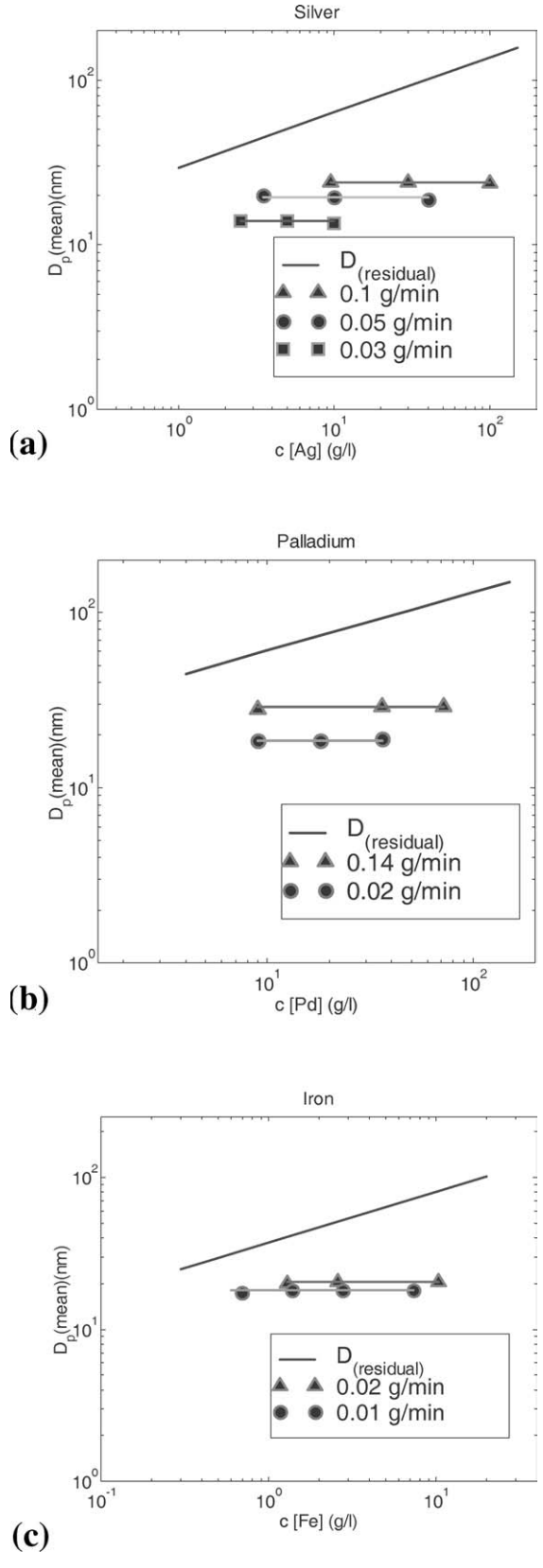

Figure 5 Geometric mean diameter of particles as a function of metal mass concentration in precursor. Sets of runs with constant mass flow rates (a) Ag ($\dot{m} = 0.03$, 0.05 and 0.1 g/min), (b) Pd ($\dot{m} = 0.02$ and 0.14 g/min) and (c) Fe ($\dot{m} = 0.01$ and $m = 0.02$ g/min). For comparison, the hypothetical curve for calculated residual particle size is also shown in each graph.

geometric number mean diameters in the range 10–50 nm. The geometric standard deviation of the generated size distributions is small, in the range of 1.35–1.5. Log-normal distributions were fitted into these measured size distributions. The given results

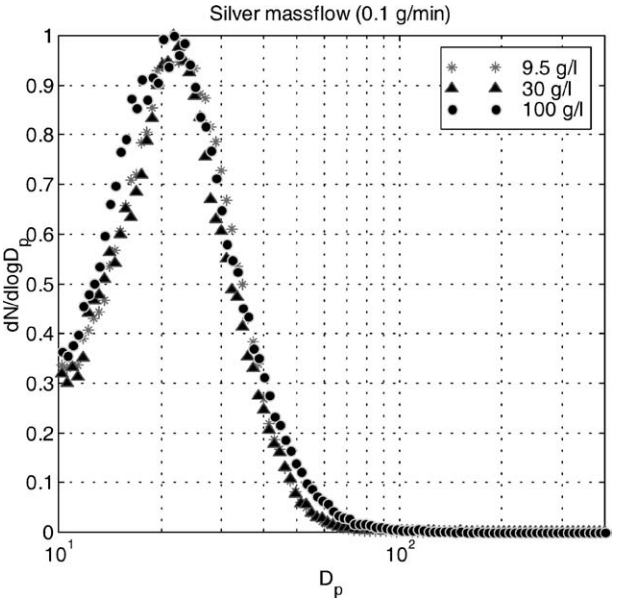

Figure 6 Three examples of number size distributions (normalised $dN/d\log D_p$) for generated silver particles with identical mass flow rate of 0.1 g/min for the metal, but for different liquid feed rate and precursor concentration in the solvent.

for particle size are the geometric number mean diameters obtained from the fitting procedure. In all the distributions, the nucleation mode contributed for 80–100% of the total mass of the particles.

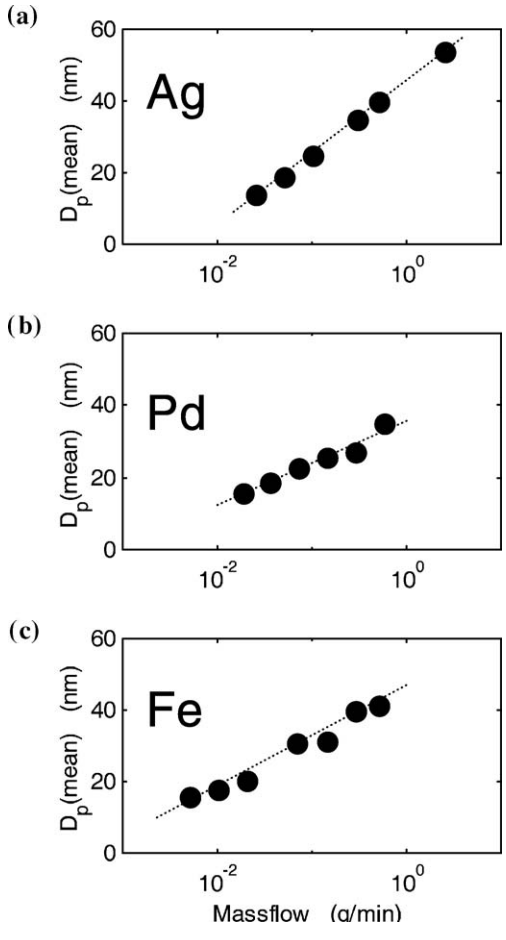

Figure 7 Geometric (number) mean diameters of the generated particles for different compounds as a function of metal mass flow rate. Each value presents an average of ca. 3–10 measurements: (a) Silver, (b) Palladium, and (c) Iron.

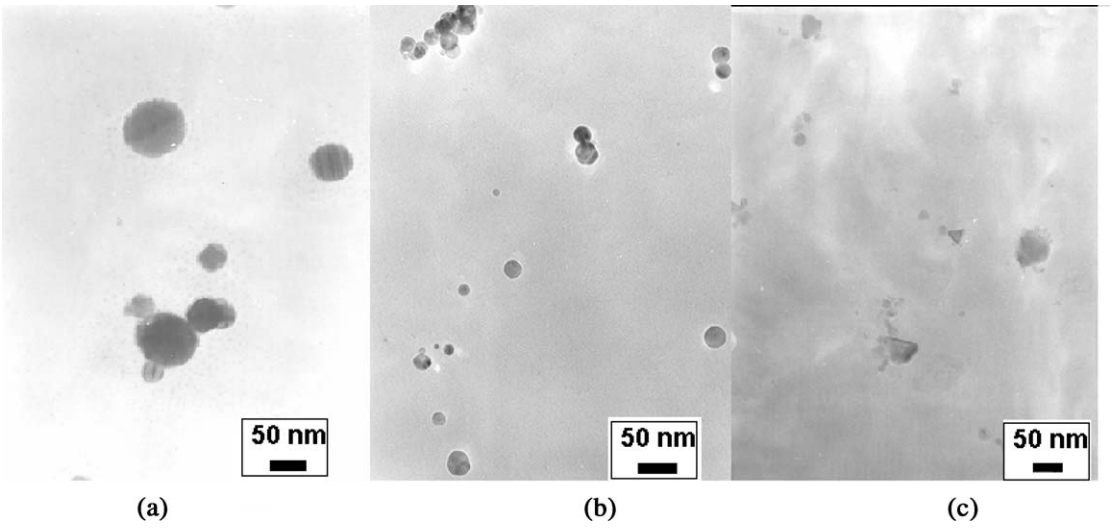

Figure 8 TEM micrographs of three samples (a) Ag ($\dot{m} = 2.5$ g/min), (b) Pd ($\dot{m} = 0.26$ g/min) and (c) Fe ($\dot{m} = 0.26$ g/min). The corresponding geometric mean diameters from Fig. 7a–c are ∼55 nm (Ag), ∼25 nm (Pd) and ∼40 nm (Fe).

Both metal precursor concentration in precursor, c, and liquid feed rate, q, were seen to have an effect on the particle size. As a general trend, with an increasing c and a constant q, the particle size was seen to increase. Also a constant c but an increasing q resulted in increasing particle size. Therefore, runs with constant mass flow rate ($\dot{m} = cq$) but varying c and q were performed.

Fig. 5a shows results from three sets of runs with constant Ag mass flow rates of 0.03, 0.05 and 0.1 g/min. The geometric mean diameters, determined from the fitting procedure and averaged over 3–10 individual spectra, have been plotted here as a function of precursor mass concentration in the liquid. For each value of Ag mass flow rate, the mean particle size stays constant, i.e., each set creates a horizontal line in Fig. 5a. The size of the dot was chosen to be representative of the error estimate and the approximate amount of variation within the set. For comparison, a hypothetical curve for calculated residual particle size is also shown. The residual size was calculated using precursor concentration and wet droplet size values. The latter was measured by laser diffractometry without a flame. A higher precursor concentration would produce a larger residual particle. The measured data clearly disagree with the calculated residual size. There is no dependency on the precursor concentration in the liquid. Furthermore, within each set the particle size stays constant. This is true also for Fe and Pd (Fig. 5b and c). As an example, three spectra from the set with $\dot{m} = 0.1$ g/min but with precursor concentrations of 9.5, 30 and 100 g/l are shown in Fig. 6. Not only the mean size of the spectra but also the shape of the size distribution remains unchanged.

Fig. 7a–c show semi-log graphs of the measured geometric mean diameter of aerosol particles as a function of metal mass flow rate for the three compounds: The mean particle size is directly proportional to the logarithm of metal mass flow rate. The same trend was already seen in Fig. 5a–c where, with an increasing mass flow rate of metal, larger mean particle sizes were obtained. In Fig. 7a–c it can now be seen that the

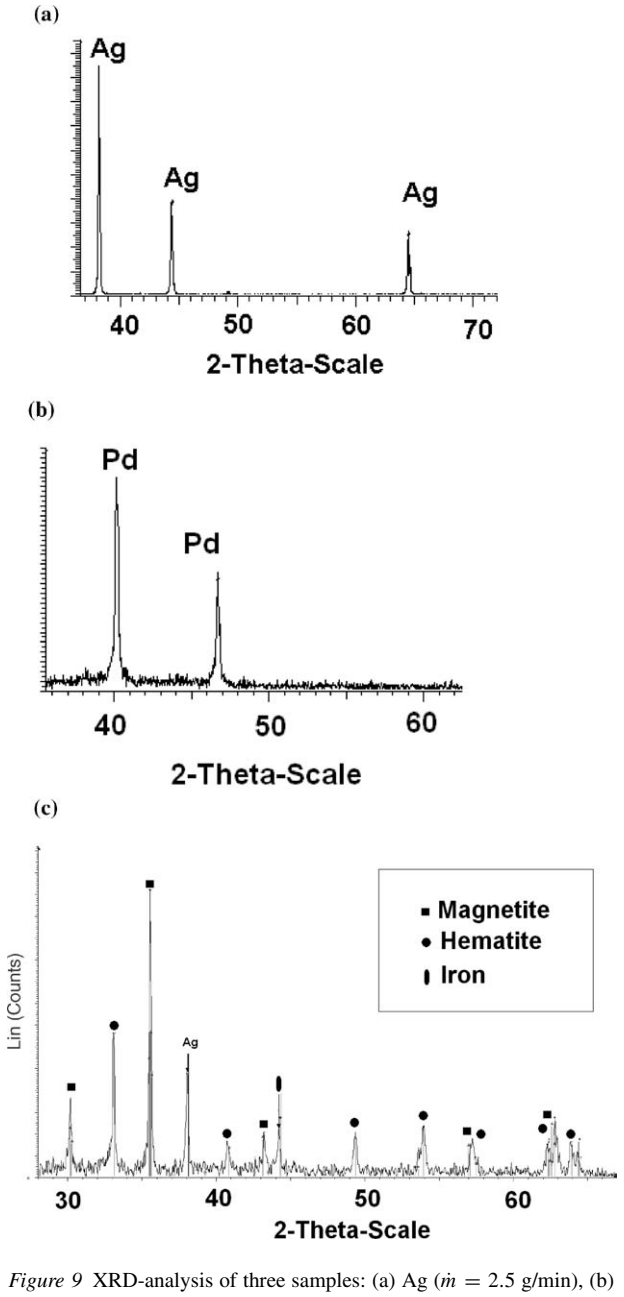

Figure 9 XRD-analysis of three samples: (a) Ag ($\dot{m} = 2.5$ g/min), (b) Pd ($\dot{m} = 0.6$ g/min), and (c) Fe ($\dot{m} = 0.6$ g/min).

dependency of the mean particle size on the metal mass flow rate is systematic.

3.2. Particle morphology

The studies on particle morphology by TEM show that Ag and Pd particles are spherical and only slightly agglomerated (Fig. 8a and b). Fe particles, however, are slightly agglomerated and some of them are non-spherical as shown in Fig. 8c. The crystalline structure of the particles for all the compounds was verified by diffraction.

The density of the particles in the gas phase can be determined by a standard aerosol measurement technique. Simultaneous measurement by both SMPS and ELPI gives an approximate value for the density of the particles [16]. In a previous work [16], an effective density of 10.58 g/cm^3 for silver was obtained. The bulk density of silver is 10.5 g/cm^3, indicating that the silver particles consist of pure metal and are close to spherical shape. This is in agreement with TEM-micrographs.

The X-ray diffraction pattern of silver particles produced by spraying silver nitrate, shown in Fig. 9a, contains peaks corresponding to pure silver. Palladium particles were also seen to consist of pure palladium as indicated by XRD in Fig. 9b. For the iron, the XRD diffraction pattern is more complicated (Fig. 9c). The iron particles consist of three different compounds: two oxide phases, hematite Fe_2O_3 and magnetite Fe_3O_4, and pure iron. One silver peak appears in the iron-spectrum because there was some silver remaining in the collecting base.

4. Conclusions

The particle formation mechanism and particle morphology in the liquid flame spray process for generating nanoparticles have been studied. The final size (mobility size) of the generated particles could be consistently set to a value between 10 and 60 nm. Since the final particle size was observed to be a function of the mass flow rate of the metal salt precursor as well as of the mass flow rate of the pure metal, and not directly a function of the liquid feed rate or precursor concentration in the solvent, it can be concluded that at one particular stage of the process, the compound is mostly in gaseous form, either as a pure metal or as an oxide compound. Thus, the process under investigation differs from the conventional spray pyrolysis techniques.

In the study, mass flow rates of 0.003–2.0 g/min for pure metals were used. Analysis using XRD showed that both Ag and Pd remained as pure metals. Furthermore, in TEM micrographs mostly separate nanoparticles and no agglomerates were seen. With the third compound, iron, agglomerates were detected and particles were seen to consist of pure Fe, hematite (α-Fe_2O_3) and magnetite (Fe_3O_4). All the properties under study, i.e., composition, particle size and size dependency on the precursor mass flow rate indicated that all the material had been formed via gas-to-particle conversion. For all the three compounds under study, no traces of the original solute were seen to remain in the particles.

Thus, the cost effective LFS-process for generating rather monodisperse, high quality nanoparticles has been shown to operate quite reliably for single metal compound systems. The presence of multiple oxides in the case of iron has to be considered a drawback for some base metal compounds. Also high vapour pressure compounds may be difficult to deal with. Furthermore, also multicomponent systems, considered for future studies, are assumed to be a challenge for this method.

Acknowledgements

The authors wish to thank the Finnish companies Dekati, EcoCat (formerly Kemira Metalkat) and Liekki for constructive co-operation during the study, and Dr. M. Vippola for TEM-graphs. The financial support of Tekes (The National Technology Agency, Project No. 1148/401/99) is also gratefully acknowledged.

References

1. A. S. EDELSTEIN and R. C. CAMMARATA (eds.), "Nanomaterials: Synthesis, Properties and Applications" (Institute of Physics Publishing, Bristol, UK, 1996).
2. F. E. KRUIS, H. FISSAN and A. PELED, *J. Aerosol Sci.* **29** (1998) 511.
3. T.T. KODAS and M.J. HAMPDEN-SMITH, "Aerosol Processing of Materials" (Wiley-VCH, New York, 1999).
4. A. GURAV, T. KODAS, T. PLYUM and Y. XIONG, *Aerosol Sci. Technol.* **19** (1993) 411.
5. D. J. CRAIK, "Magnetic Oxides" (John-Wiley & Sons, New York, 1975).
6. M. V. CABANAS, J. M. CONZALEZ-CALBET and M. VALLET-REGI, *Ceramics: Charting the Future.* (1995) 1221.
7. J. TIKKANEN, K. A. GROSS, C. C. BERNDT, V. PITKÄNEN, J. KESKINEN, S. RAGHU, M. RAJALA and J. KARTHIKEYAN, *Surf. Coatings Technol.* **90** (1997) 210.
8. K. A. GROSS, J. TIKKANEN, J. KESKINEN, V. PITKÄNEN, M. EEROLA, R. SIIKAMÄKI and M. RAJALA, *J. Thermal Spray Technol.* **8** (1999) 583.
9. J. KARTHIKEYAN, C. C. BERNDT, J. TIKKANEN, S. REDDY and H. HERMAN, *Nanostruct. Mater.* **8** (1997a) 61.
10. J. KARTHIKEYAN, C. C. BERNDT, J. TIKKANEN, J. Y. WANG, A. H. KING and H. HERMAN, *ibid.* **9** (1997b) 137.
11. "CRC Handbook of Chemistry and Physics" 60th ed. (The Chemical Rubber Co., Cleveland, OH, 1979).
12. J. TIKKANEN, M. EEROLA, V. PITKÄNEN and M. RAJALA, "Method and Equipment for Spraying Material" Patent no. 98832-Finland (in Finnish), 1997.
13. W. KOCH, H. LÖDDING, W. MÖLTER and F. MUNZINGER, *Staub-Reinhaltung der Luft* **48** (1988) 341.
14. J. KESKINEN, K. PIETARINEN and M. LEHTIMÄKI, *J. Aerosol Sci.* **23** (1992) 353.
15. S. C. WANG and R. C. FLAGAN, *Aerosol Sci. Technol.* **13** (1990) 230.
16. J. RISTIMÄKI, A. VIRTANEN, M. MARJAMÄKI, A. ROSTEDT and J. KESKINEN, *J. Aerosol Sci.* **33** (2002) 1541.
17. Y.-S. CHENG, H.-C. YEH and G. M. KANAPILLY, *Amer. Ind. Hygiene Ass.* **42** (1981) 605.

Received 4 April 2003
and accepted 15 January 2004